Anisotropic Thermal Conductivity of 4H and 6H Silicon Carbide Measured Using Time-Domain Thermoreflectance

Xin Qian, Puqing Jiang, and Ronggui Yang*

Department of Mechanical Engineering

University of Colorado, Boulder, CO 80309, USA

Abstract

Silicon carbide (SiC) is a wide bandgap (WBG) semiconductor with promising applications in high-power and high-frequency electronics. Among its many useful properties, the high thermal conductivity is crucial. In this letter, the anisotropic thermal conductivity of three SiC samples, n-type 4H-SiC (N-doped 1×10^{19} cm^{-3}), unintentionally doped (UID) semi-insulating (SI) 4H-SiC, and SI 6H-SiC (V-doped 1×10^{17} cm^{-3}), is measured using femtosecond laser based time-domain thermoreflectance (TDTR) over a temperature range from 250 K to 450 K. We simultaneously measure the thermal conductivity parallel to (k_r) and across the hexagonal plane (k_z) for SiC by choosing the appropriate laser spot radius and the modulation frequency for the TDTR measurements. For both k_r and k_z, the following decreasing order of thermal conductivity value is observed: SI 4H-SiC > n-type 4H-SiC > SI 6H-SiC. This work serves as an important benchmark for understanding thermal transport in WBG semiconductors.

Excellent properties of silicon carbide (SiC) including its high electron mobility,[1-2] wide electronic bandgap,[3-4] and superior chemical stability [5] have led to its promising applications in high-power and high-frequency electronics, such as white light emitting diodes (LEDs),[6-8] high electron mobility transistors (HEMTs),[9-11] and high power transmissions.[12-13] Among its many useful properties, thermal conductivity is critical for the stable performance and safe operation of SiC devices at high temperatures, high frequency, and high voltages. While the thermal conductivity of SiC has been reported previously,[14-21] conflicting data still exists among different works. For example, it remains controversial whether the thermal conductivity of 4H phase of SiC is higher than that of the 6H phase.[15, 19-20] More importantly, while the anisotropy in the thermal conductivity of both 4H- and 6H- SiC is expected due to their hexagonal Bravais lattice structures (as shown in Figure 1a), it has usually been ignored in previous experimental studies[14, 17-18] due to the challenges in accurate measurements. So far, there is only one experimental work[16] reporting the anisotropic thermal conductivity of 6H-SiC measured using photothermal radiometry, which shows that the cross-plane thermal conductivity k_z (perpendicular to the hexagonal planes) of 6H-SiC is 30% lower than its in-plane thermal conductivity k_r (parallel to the hexagonal planes). The anisotropic thermal conductivity of 4H-SiC has not been systematically studied experimentally.

In this paper, we use the time-domain thermoreflectance (TDTR)[22] to simultaneously determine both the k_r and k_z of three SiC single crystals provided by II-VI Inc.®: unintentionally doped (UID) semi-insulating (SI) 4H-SiC, n-type 4H-SiC (N-doped 1×10^{19} cm^{-3}), and SI 6H-SiC (V-doped 1×10^{17} cm^{-3}), over a temperature range from 250 K to 450 K. Anisotropy is observed in thermal conductivity of all the SiC samples, with k_z ~40% lower than k_r. For both k_z and k_r, the measured thermal conductivity has the following decreasing order: SI 4H-SiC > n-type 4H-SiC > 6H, which agrees well with the recent first principles predictions by Protik *et al.*[19]

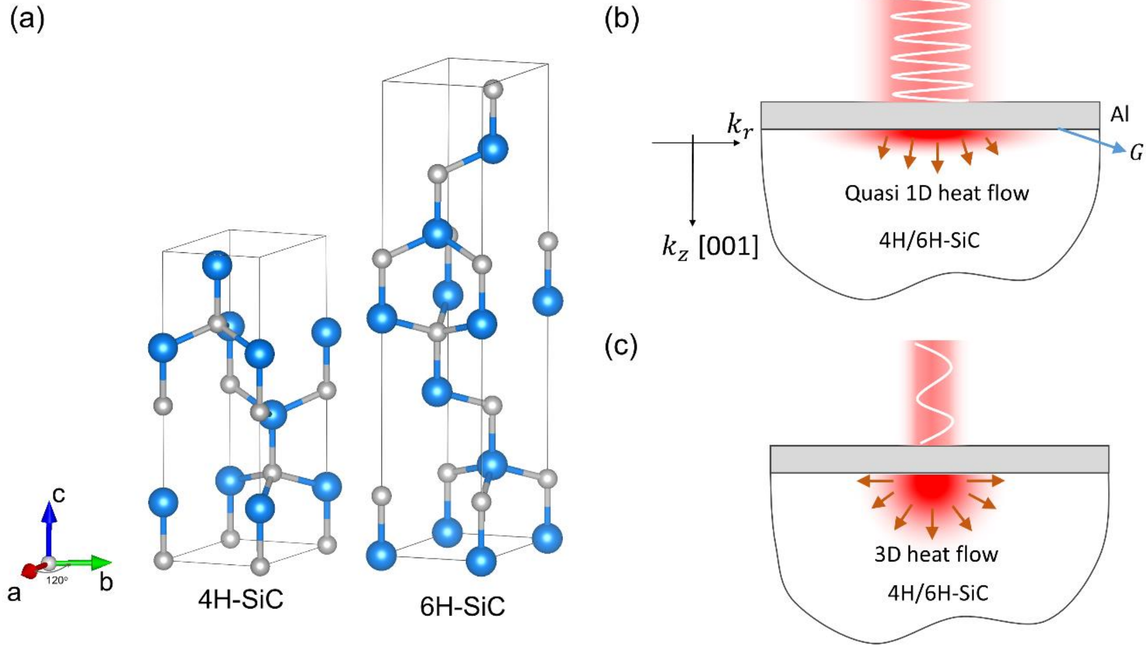

Figure 1. (a) Atomic structure of 4H-SiC and 6H-SiC. (b) Schematic for measuring k_z using a large spot size and a high modulation frequency of TDTR measurements. (c) Schematic for measuring k_r using a small spot size and a low modulation frequency of TDTR measurements.

We measure the anisotropic thermal conductivity k_r and k_z using TDTR by varying the laser spot size and the modulation frequency,[23] as shown in Figure 1b-c, where a ~110 nm Al transducer was deposited on all SiC samples. In TDTR measurement, the surface heating by the laser is transient and non-uniform with a Gaussian profile. Although the heat conduction with such transient Gaussian heating as boundary condition can be fully solved in the cylindrical coordinates,[24] it is still necessary to understand how to appropriately choose the experimental parameters for separate measurement of the anisotropic thermal conductivity k_r and k_z. There are two important length scales in the TDTR experiments that determine the heat flow direction in the SiC substrate and hence the different sensitivities to k_r and k_z. The first length scale is the size of the Gaussian laser spot, defined as the root-mean-square average of the $1/e^2$ radii of the pump (w_0)

and the probe (w_1) as: $w = \sqrt{(w_0^2 + w_1^2)/2}$. The other important length scale is the thermal penetration length:

$$d_{P,\alpha} = \sqrt{k_\alpha / C\pi f_0} \tag{1}$$

where the subscript $\alpha(= r, z)$ denotes the direction in cylindrical coordinates, k is the thermal conductivity, and C is the volumetric heat capacity. Since TDTR measures the surface temperature rise within the RMS radius of the laser spot, whether the TDTR signal is sensitive to k_r depends on how large the laser spot radius w is compared to the in-plane thermal diffusion length $d_{P,r}$. If the spot radius w is much larger than the in-plane penetration length $d_{P,r}$, the in-plane temperature gradient is negligible and the heat flow can be regarded as one-dimensional along the cross-plane direction. Based on our previous work, the criterion for satisfying the quasi one-dimensional thermal transport along the cross-plane direction is: [23]

$$w \geq 5 d_{P,r} \tag{2}$$

By satisfying Eq. (2), the TDTR signal is only sensitive to the parameters associated with cross-plane heat transfer, namely, the cross-plane thermal conductivity k_z and the interface conductance G between the transducer and the SiC substrate. After determining k_z and G, k_r can then be measured reliably if the laser spot radius is chosen to satisfy the condition that the in-plane penetration length $d_{P,r}$ is at least half of the laser spot radius:[23]

$$d_{P,r} \geq \frac{1}{2} w \tag{3}$$

In principle, both the modulation frequency f_0 and the laser spot radius w can be varied to separately measure k_r and k_z.[25] For example, k_z could be first measured using a large spot radius w at a high modulation frequency f_0 (as shown in Figure 1b), then k_r can be measured using a

small spot radius w at a low modulation frequency (as shown in Figure 1c). However, we need to be cautious that the measured k_z could depend on f_0 when different phonon modes are out of thermal equilibrium [26-31] and k_r could be underestimated if w_0 is smaller than the mean free paths of heat carrying phonons.[29, 32-34]

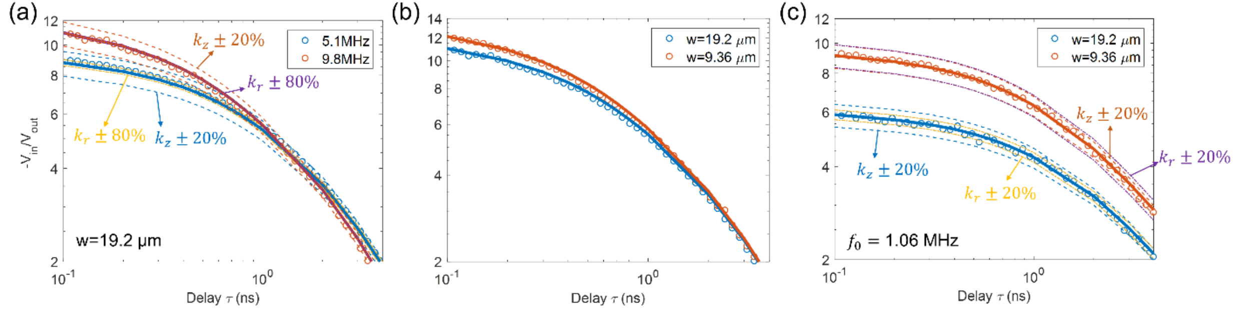

Figure 2. (a) Measurement of cross-plane thermal conductivity k_z of SI 6H-SiC sample at room temperature with $f_0 = 5.1$ MHz and 9.8 MHz where the TDTR signal has negligible sensitivity to k_r. The best parameters are $k_z = 273$ W/mK and $G = 128$ MW/m^{2}K. (b) The best-fit (k_z, G) obtained using $w = 19.2$ μm can also fit the TDTR signal using a smaller spot radius $w = 9.4$ μm, indicating k_z and G are independent of laser spot size. (c) Measurement of in-plane thermal conductivity k_r at low modulation frequency at $f_0 = 1.06$ MHz. Using both $w = 9.4$ μm and $w = 19.2$ μm, the obtained in-plane thermal conductivity is the same $k_r = 393$ W/mK.

We perform the following measurements to make sure that the measured thermal conductivity of SiC samples is intrinsic and is not affected by the choices of operation parameters such as the laser spot radius or the modulation frequency. First, we check whether k_z depends on f_0 by using a large spot radius w = 19.2 μm. Using the in-plane thermal conductivity k_r from first principles[19] calculation and heat capacity C taken from ref [[35]], we estimate from Eq. (2) that the modulation frequency f_0 should be higher than 4.6 MHz for the independent measurement of k_z. We thus conduct the measurements for k_z at two different modulation frequencies of $f_0 = 5.1$ MHz and 9.8 MHz, with the obtained signals shown in Figure 2a. It is clear that the obtained signal can be regarded as independent of k_r. To fit the experimental signal, nonlinear least-squares regression is used in this work. The cost function for the regression is defined as:

$$W(\boldsymbol{U}) = \sum_{j}\sum_{i}\left[R_{Exp}\left(\tau_i, f_{0j}\right) - F(\tau_i, f_{0j}, \boldsymbol{U}, \boldsymbol{P})\right]^2 \tag{4}$$

where $R_{Exp}\left(\tau_i, f_{0j}\right)$ is the ratio $-V_{in}/V_{out}$ between the in-phase signal V_{in} and the out-of-phase signal V_{out} measured at delay time τ_i and modulation frequency f_{0j}, and the function F denotes the full solution of heat conduction equation with periodic Gaussian heating profile as the boundary condition, which is used to predict $-V_{in}/V_{out}$. We note that the ratio $-V_{in}/V_{out}$ is essentially equivalent to the phase ϕ of the signal since $\tan\phi = V_{out}/V_{in}$. The vector $\boldsymbol{P}$ is the set of control parameters including the thickness, heat capacity and thermal conductivity of the Al transducer, as well as the laser spot radius. The vector $\boldsymbol{U} = [k_r, k_z, G]^{\mathrm{T}}$ is a set of unknown parameters that need to be determined during the nonlinear regression, where G is the interface conductance between the SiC and the Al transducer. As discussed above, since k_r has negligible effect on the predicted ratio $-V_{in}/V_{out}$ when Eq. (2) is satisfied, U can be reduced to $\boldsymbol{U} = [k_z, G]$ and k_r is set equal to k_z during the nonlinear regression. Using the simplex algorithm,[36] the unknown parameters $\boldsymbol{U}$ are adjusted iteratively, until the change of an element in $\boldsymbol{U}$ and the reduction of W between the succeeding steps are both smaller than 0.1%. Using the nonlinear regression, we found that the signals obtained at 5.1 MHz and 9.8 MHz can be fitted with the same value of k_z and G, indicating that the cross-plane thermal transport in SiC is not affected by the modulation frequency. We then performed the measurement for k_z at the same modulation frequency of $f_0 = 9.8$ MHz using different spot radii of w = 19.2 µm and 9.36 µm, which yield the same k_z, indicating that the cross-plane thermal conductivity k_z is not affected by the spot radius w either, as shown in Figure 2b.

After making sure that k_z and G are not affected by f_0 or w, we proceed to measure the in-plane thermal conductivity k_r. Using Eq. (3), we determine that the modulation frequency should

be $f_0 \leq 2.9$ MHz to ensure that the measured signal is sensitive to k_r when we use the spot radius $w = 9.4$ µm. We therefore select $f_0 = 1.06$ MHz to measure k_r, as shown in Figure 2c. Similar to the cross-plane thermal conductivity measurement, we use the same nonlinear regression algorithm, but the unknown parameter $\boldsymbol{U} = k_r$ in this case, and k_z and G are regarded as known parameters by grouping them into $\boldsymbol{P}$. We then repeated the measurement described above but with a larger spot radius $w = 19.2$ µm to make sure the w is large enough so that k_r reaches the diffusive limit. We found the k_r measured using $w = 9.4$ µm can successfully fit the TDTR signal obtained with $w = 19.2$ µm, indicating the measured k_r is already converged with respect to w. Based on the first-principles calculation,[19] the mean free paths of heat carrying phonons are estimated to be in the range 1~12 µm at room temperature. The smallest diameter of we use in our measurement $2w$ =18.8 µm is still larger than the longest phonon mean free paths, and the ballistic effect induced by the limited laser spot size should be negligible. Through the above measurements, we are confident that both k_r and k_z of 6H-SiC are intrinsic values, free of any extra error induced by ballistic transport or non-equilibrium transport. We performed similar measurements on SI and n-type 4H-SiC samples, and we obtained robust k_r and k_z independent of the modulation frequency and the laser spot radius. In the rest of the paper, we therefore measure k_z at $f_0 = 9.8$ MHz and k_r at f_0 =1.06 MHz for all the SiC samples using the same spot radius $w = 9.4$ µm.

The discussion above suggests that the unknown parameters $\boldsymbol{U} = [k_r,\ k_z, G]^{\mathrm{T}}$ can be simultaneously determined through fitting the signal obtained at $f_0 = 1.06$ MHz and 9.8 MHz at the same spot radius $w = 9.4$ µm. Since we are measuring multiple parameters at multiple modulation frequencies, an error propagation formula based on the least-squares regression is necessary. We extended the error propagation formula by Yang *et al.*[37] in our previous work for

the case when multiple modulation frequencies are used.[31] The error propagation formula is written as:

$$var[\boldsymbol{U}] = \boldsymbol{\Sigma}_{\boldsymbol{U}}^{-1}\left[\sum_{j} \boldsymbol{J}_{\boldsymbol{U}}^{\mathrm{T}}(f_{0j}) var[\boldsymbol{R}_{Exp}(f_{0j})] \boldsymbol{J}_{\boldsymbol{U}}(f_{0j})\right]\boldsymbol{\Sigma}_{\boldsymbol{U}}^{-1} + \boldsymbol{\Sigma}_{\boldsymbol{U}}^{-1}\boldsymbol{\Sigma}_{\boldsymbol{UP}} var[\boldsymbol{P}]\boldsymbol{\Sigma}_{\boldsymbol{UP}}^{\mathrm{T}}\boldsymbol{\Sigma}_{\boldsymbol{U}}^{-1} \quad (5)$$

where $var[\cdot]$ denotes the covariance matrix, $\boldsymbol{R}_{Exp}(f_{0j}) = \left[-\frac{V_{in}}{V_{out}}(\tau_1, f_{0j}), \dots, -\frac{V_{in}}{V_{out}}(\tau_i, f_{0j}), \dots\right]^{\mathrm{T}}$ is the vector containing the TDTR ratio between in-phase signal V_{in} and out-of-phase signal V_{out} measured at a sequence of delay time $[\tau_1, \tau_2, \dots, \tau_i, \dots]^{\mathrm{T}}$ and modulation frequency f_{0j}, and, $\boldsymbol{P}$ is the vector containing input parameters including the rms laser spot radius w, thickness d_{Al}, heat capacity C_{Al} and thermal conductivity k_{Al} of the transducer, and the heat capacity C of SiC. The $\boldsymbol{\Sigma}$ matrices in Eq. (5) are written as:

$$\boldsymbol{\Sigma}_{\boldsymbol{U}} = \sum_{j} \boldsymbol{J}_{\boldsymbol{U}}^{\mathrm{T}}(f_{0j})\boldsymbol{J}_{\boldsymbol{U}}(f_{0j}), \qquad \boldsymbol{\Sigma}_{\boldsymbol{UP}} = \sum_{j} \boldsymbol{J}_{\boldsymbol{U}}^{\mathrm{T}}(f_{0j})\boldsymbol{J}_{\boldsymbol{P}}(f_{0j}) \quad (6)$$

where $\boldsymbol{J}_{\boldsymbol{U}}(f_{0j}) = \left.\frac{\partial(F(\tau_1),F(\tau_2),\dots,F(\tau_i),\dots)}{\partial(k_r,k_z,G)}\right|_{f_{0j}}$ and $\boldsymbol{J}_{\boldsymbol{P}}(f_{0j}) = \left.\frac{\partial(F(\tau_1),F(\tau_2),\dots,F(\tau_i),\dots)}{\partial(w,d_{Al},C_{Al},k_{Al},C)}\right|_{f_{0j}}$ are the Jacobi matrices of the thermal model F with respect to $\boldsymbol{U}$ and $\boldsymbol{P}$ at frequency f_{0j}, respectively. The diagonal elements in the $var[\boldsymbol{U}\ or\ \boldsymbol{P}]$ are essentially the variance σ^2 of the parameters, and we use 2σ as the uncertainty reported in this paper. The uncertainties (2σ) of the control parameters $\boldsymbol{P}$ are estimated as follows: 10% for the thermal conductivity of Al, 5% for the heat capacity of Al and the substrate, 5% for the Al thickness, and 4% for the laser spot size.[23, 31] We summarize the calculated $4 \cdot var[\boldsymbol{U}]$ for the SI 4H-SiC, n-type 4H-SiC and SI 6H-SiC in Table 1, so that the uncertainties 2σ can be directly calculated as square root of the diagonal elements.

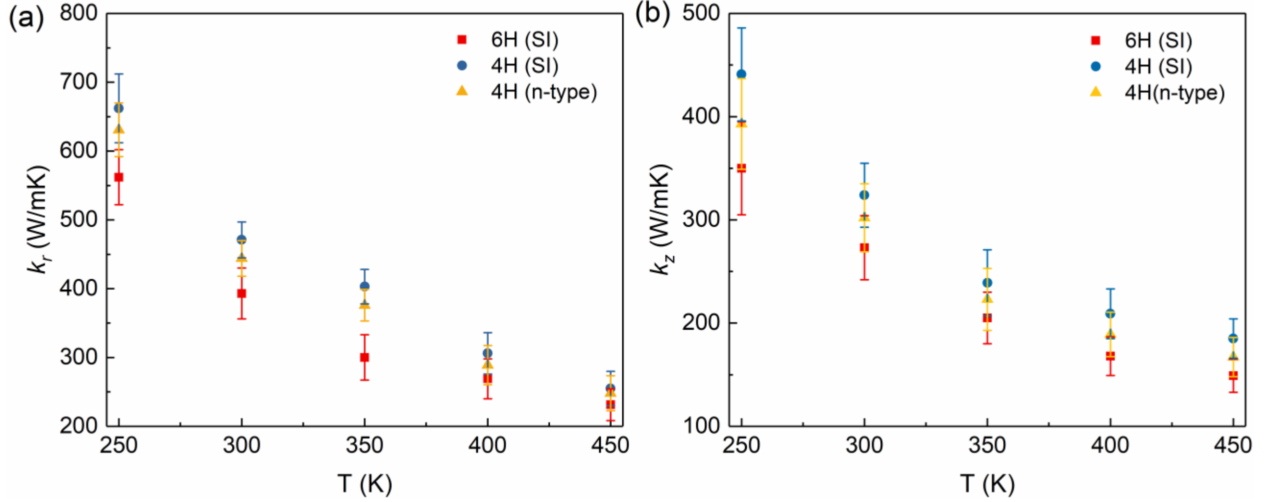

Figure 3. Temperature-dependent thermal conductivity of SI 4H SiC, n-type 4H SiC ,and SI 6H SiC in (a) the in-plane direction and (b) the cross-plane direction.

Figure 3 summarizes the temperature-dependent k_r and k_z for the SI 4H-SiC, n-type SiC, and SI 6H-SiC from 250 K to 450 K. Anisotropy is clearly observed in the measured thermal conductivity for all three SiC samples from 250 K to 450 K, with k_z about 40% lower than k_r. The SI and n-type 4H-SiC have higher k_r and k_z than those of SI 6H-SiC sample, which agree well with the first principles predictions that the thermal conductivity of nH-SiC (n = 2, 4, 6) decreases with increasing n.[19] The SI 4H-SiC has the highest thermal conductivity among the three SiC crystals, with 7% higher thermal conductivity than the n-type 4H-SiC due to the phonon-impurity scattering in n-type 4H SiC. Figure 4 shows the interface conductance between the Al transducer and the three SiC samples. Because of the high Debye temperature of SiC (4H 1300 K and 6H 1200 K),[38] the interface conductance of three samples increases as the temperature rises from 250 K to 450 K. The 6H SiC has higher interface conductance with Al, because its Debye temperature is better matched with Al (433 K).[39]

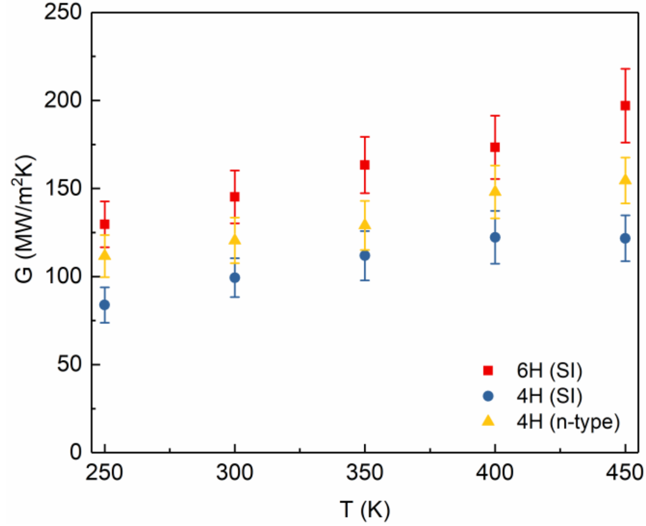

Figure 4. Interface conductance between Al transducer and the SiC samples.

Figure 5 compares our measured k_r and k_z for 4H-SiC with relevant experimental measurements and the first-principles calculation results in literature. In the in-plane direction, our results agree well with the first principles calculation,[19] but much higher than the measurement by Morelli et al.[20] The much lower thermal conductivity by Morelli *et al.* [20] is due to the defects in their 4H-SiC samples, as suggested by the authors. In the cross-plane direction, the measured k_z for SI 4H-SiC is slightly smaller than the first-principles calculations but higher than the laser flash analysis (LFA) measurements by Wei *et al.*[17] above 350 K. It is confusing that the temperature-dependent thermal conductivity measured in their work has the $1/T^2$ temperature dependence, largely deviating from the $1/T$ law.[40] In Figure 6, we compare the anisotropic thermal conductivity of SI 6H-SiC with both first principles calculations and the measurements by others. For both the k_r and k_z, our TDTR measurements agree well with the first-principles calculation[19] and measurement by others. [16, 19, 21]

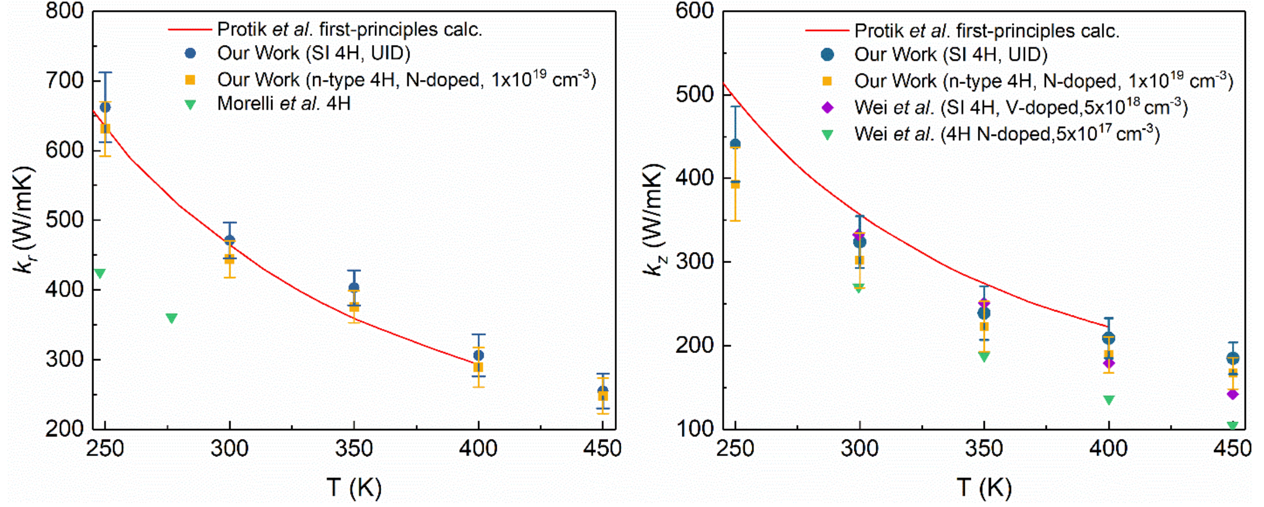

Figure 5. (a) In-plane thermal conductivity for SI and n-type 4H-SiC compared with the first-principles calculation by Protik *et al.*,[19] and the steady-state measurement by Morelli *et al.* [20] (b) The cross-plane thermal conductivity for SI and n-type 4H-SiC compared with the calculation by Protik *et al.* [19] and the laser flash analysis measurement by Wei *et al.* [17]

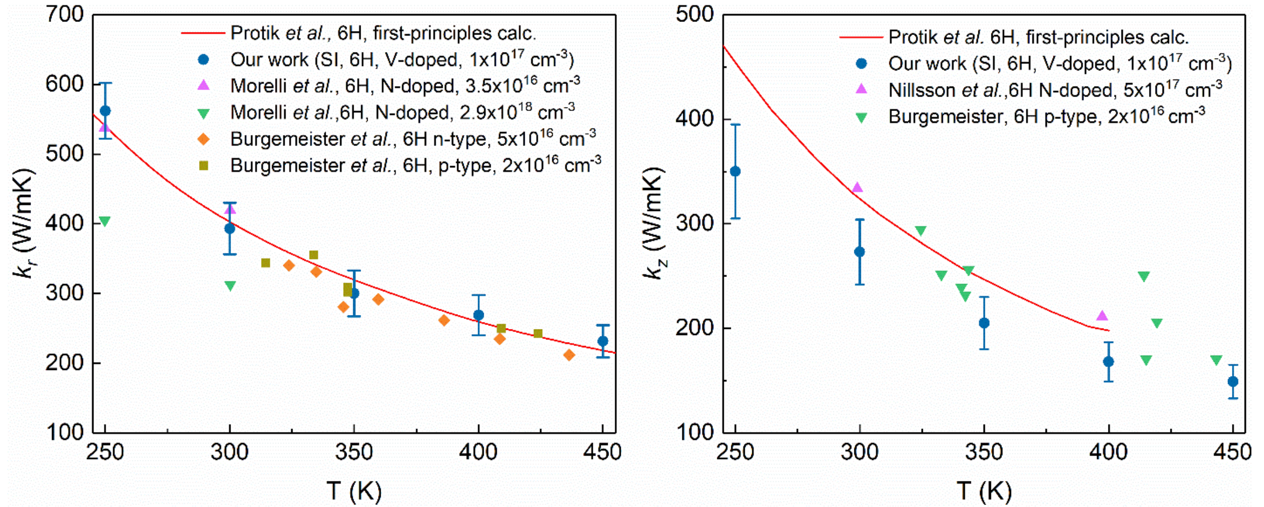

Figure 6 (a) In-plane thermal conductivity for SI 6H-SiC compared with the first-principles calculation by Protik *et al.*,[19] the steady-state measurement by Morelli *et al.*[18] and the radiation thermometry by Burgemeister *et al.*[16] (b) The cross-plane thermal conductivity for SI 6H-SiC compared with the calculation by Burgemeister *et al.*[16], Protik *et al.* ,[19] and Nilsson *et al.* [21]

In summary, we have measured both the in-plane and the cross-plane thermal conductivity of SI 4H-SiC, n-type 4H-SiC, and SI 6H-SiC using TDTR by varying both the laser spot radius and

the modulation frequency of TDTR measurements. We developed a measurement protocol to make sure that the measured thermal conductivities are intrinsic values, independent of the choices of operational parameters such as the laser spot radius and the modulation frequency. Our measurement results confirmed the first-principles prediction that thermal conductivity is anisotropic in the hexagonal SiC crystals, and that 4H-SiC has higher thermal conductivity than 6H-SiC. This work provides an important benchmark for understanding thermal transport in WBG semiconductors.

Acknowledgements. This work was supported by the NSF (Grant No. 1512776). RY acknowledges Rajan Rengarajan at II-VI Inc. and John Blevins at AFRL for providing the SiC samples and helpful discussions.

Table 1. *The covariance matrices* $4 \cdot var[k_r, k_z, G]$ *for the SiC samples at room temperature. The diagonal of the matrices shown in the table is the uncertainty level* 2σ. *The units shown for the covariance matrices are* k_r *(W/mK),* k_z *(W/mK) and* G *(MW/m*^{2}*K).*

SI 6H- SiC	k_r	k_z	G
k_r	1101	-73.7	21.3
k_z	-73.7	1267	302.2
G	21.3	302.2	94.6
Best-fit	393	273	128
Uncertainty	8.4%	13.0%	7.6%
SI 4H-SiC	k_r	k_z	G
k_r	1588.1	-372.2	26.8
k_z	-372.2	2421.0	275.8
G	26.8	275.8	53.4
Best-fit	471	324	101
Uncertainty	8.5%	15.2%	7.2%
n-type 4H-SiC	k_r	k_z	G
k_r	1315.5	-206.4	25.1
k_z	-206.4	1642.2	284.3
G	25.1	284.3	76.3
Best-fit	444	302	121
Uncertainty	8.7%	13.4%	7.3%

References:

1. Roschke, M.; Schwierz, F., Electron Mobility Models for 4h, 6h, and 3c Sic. *IEEE Trans. Electron Devices* **2001**, *48*, 1442.
2. Chung, G. Y.; Tin, C. C.; Williams, J. R.; McDonald, K.; Chanana, R. K.; Weller, R. A.; Pantelides, S. T.; Feldman, L. C.; Holland, O. W.; Das, M. K.; Palmour, J. W., Improved Inverstion Channel Mobiility for 4h-Sic Mosfects Fowlling High Temperature Anneals in Nitric Oxide. *IEEE Electron Device Letters* **2001**, *22*, 176.
3. Lambrecht, W. R. L.; Limpijumnong, S.; Rashkeev, S. N.; Segall, B., Electronic Band Structure of Sic Polytypes: A Discussion of Theory and Experiment. *Physica status solidi (b)* **1997**, *202*, 5.
4. Park, C. H.; Cheong, B.-H.; Lee, K.-H.; Chang, K. J., Structural and Electronic Properties of Cubic, 2h, 4h, and 6hsic. *Phys. Rev. B* **1994**, *49*, 4485-4493.
5. Kishimoto, H.; Katoh, Y.; Kohyama, A., Microstructural Stability of Sic and Sic/Sic Composites under High Temperature Irradiation Environment. *J. Nucl. Mater.* **2002**, *307-311*, 1130-1134.
6. Patrick, L.; Choyke, W. J., Photoluminescence of Radiation Defects in Ion-Implanted6hsic. *Phys. Rev. B* **1972**, *5*, 3253-3259.
7. Fuchs, F.; Soltamov, V. A.; Vath, S.; Baranov, P. G.; Mokhov, E. N.; Astakhov, G. V.; Dyakonov, V., Silicon Carbide Light-Emitting Diode as a Prospective Room Temperature Source for Single Photons. *Scientific reports* **2013**, *3*, 1637.
8. Zheludev, N., The Life and Times of the Led - a 100-Year History. *Nature Photonics* **2007**, *1*, 189-192.
9. Morkoç, H.; Strite, S.; Gao, G. B.; Lin, M. E.; Sverdlov, B.; Burns, M., Large‐Band‐Gap Sic, Iii‐V Nitride, and Ii‐Vi Znse‐Based Semiconductor Device Technologies. *J. Appl. Phys.* **1994**, *76*, 1363-1398.
10. Binari, S. C.; Klein, P. B.; Kazior, T. E., Trapping Effects in Gan and Sic Microwave Fets. *Proc. IEEE* **2002**, *90*, 1048.
11. Pengelly, R. S.; Wood, S. M.; Milligan, J. W.; Sheppard, S. T.; Pribble, W. L., A Review of Gan on Sic High Electron-Mobility Power Transistors and Mmics. *IEEE Trans. Microwave Theory Tech.* **2012**, *60*, 1764.
12. Peftitsis, D.; Tolstoy, G.; Antonopoulos, A.; Rabkowski, J.; Lim, J.-K.; Bakowski, M.; Angquist, L.; Nee, H.-P., High-Power Modular Multilevel Converters with Sic Jfets. *IEEE Transactions on Power Electronics* **2012**, *27*, 28.
13. Biela, J.; Schweizer, M.; Waffler, S.; Kolar, J. W., Sic Versus Si - Evaluation of Potentials for Performance Improvement of Inverter and Dc-Dc Converter Systems by Sic Power Semiconductors. *IEEE Transactions on Industrial Electronics* **2011**, *58*, 2872.
14. Slack, G. A., Thermal Conductivity of Pure and Impure Silicon, Silicon Carbide, and Diamond. *J. Appl. Phys.* **1964**, *35*, 3460-3466.
15. Brethauer, J., *Mapping the Thermal Conductivity of Sic/Sic Composites, Phd Thesis*; University of Illinois at Urbana-Champaign, 2017.
16. Burgemeister, E. A.; von Muench, W.; Pettenpaul, E., Thermal Conductivity and Electrical Properties of 6hsilicon Carbide. *J. Appl. Phys.* **1979**, *50*, 5790-5794.
17. Wei, R.; Song, S.; Yang, K.; Cui, Y.; Peng, Y.; Chen, X.; Hu, X.; Xu, X., Thermal Conductivity of 4h-Sic Single Crystals. *J. Appl. Phys.* **2013**, *113*, 053503.
18. Morelli, D. T.; Heremans, J. P.; Beetz, C. P.; Yoo, W. S.; Matsunami, H., Phonon‐Electron Scattering in Single Crystal Silicon Carbide. *Appl. Phys. Lett.* **1993**, *63*, 3143-3145.
19. Protik, N. H.; Katre, A.; Lindsay, L.; Carrete, J. u.; Mingo, N.; Broido, D., Phonon Thermal Transport in 2h, 4h, and 6h Silicon Carbide from First Principles. *Materials Today Physics* **2017**, *1*, 31-38.
20. Morelli, D. T.; Heremans, J. P.; Beetz, C. P.; Yoo, W. S.; Harris, G.; Taylor, C., Carrier Concentration Dependence of the Thermal Conductivity of Silicon Carbide. *Institute of Physics Conference Series* **1994**, *137*, 313-316.

21. Nilsson, O.; Mehling, H.; Horn, R.; Fricke, J.; Hofmann, R.; M¨uller, S. G.; Eckstein, R.; Hofmann, D., Determination of the Thermal Diffusivity and Conductivity of Monocrystalline Silicon Carbide (300-2300 K). *High Temperatures . High Pressures* **1997**, *29*, 73-79.
22. Zhu, J.; Tang, D.; Wang, W.; Liu, J.; Holub, K. W.; Yang, R., Ultrafast Thermoreflectance Techniques for Measuring Thermal Conductivity and Interface Thermal Conductance of Thin Films. *J. Appl. Phys.* **2010**, *108*, 094315.
23. Jiang, P.; Qian, X.; Yang, R., Time-Domain Thermoreflectance (Tdtr) Measurements of Anisotropic Thermal Conductivity Using a Variable Spot Size Approach. *Rev. Sci. Instrum.* **2017**, *88*, 074901.
24. Cahill, D. G., Analysis of Heat Flow in Layered Structures for Time-Domain Thermoreflectance. *Rev. Sci. Instrum.* **2004**, *75*, 5119-5122.
25. Liu, J.; Zhu, J.; Tian, M.; Gu, X.; Schmidt, A. J.; Yang, R., Simultaneous Measurement of Thermal Conductivity and Heat Capacity of Bulk and Thin Film Materials Using Frequency-Dependent Transient Thermoreflectance Method. *Rev. Sci. Instrum.* **2013**, *84*, 034902.
26. Koh, Y. K.; Cahill, D. G., Frequency Dependence of the Thermal Conductivity of Semiconductor Alloys. *Phys. Rev. B* **2007**, *76*.
27. Koh, Y. K.; Cahill, D. G.; Sun, B., Nonlocal Theory for Heat Transport at High Frequencies. *Phys. Rev. B* **2014**, *90*.
28. Sun, B.; Gu, X.; Zeng, Q.; Huang, X.; Yan, Y.; Liu, Z.; Yang, R.; Koh, Y. K., Temperature Dependence of Anisotropic Thermal-Conductivity Tensor of Bulk Black Phosphorus. *Adv. Mater.* **2017**, *29*.
29. Wilson, R. B.; Cahill, D. G., Anisotropic Failure of Fourier Theory in Time-Domain Thermoreflectance Experiments. *Nature communications* **2014**, *5*, 5075.
30. Wilson, R. B.; Feser, J. P.; Hohensee, G. T.; Cahill, D. G., Two-Channel Model for Nonequilibrium Thermal Transport in Pump-Probe Experiments. *Phys. Rev. B* **2013**, *88*.
31. Jiang, P.; Qian, X.; Gu, X.; Yang, R., Probing Anisotropic Thermal Conductivity of Transition Metal Dichalcogenides Mx2 (M = Mo, W and X = S, Se) Using Time-Domain Thermoreflectance. *Adv. Mater.* **2017**, *29*, 1701068.
32. Ding, D.; Chen, X.; Minnich, A. J., Radial Quasiballistic Transport in Time-Domain Thermoreflectance Studied Using Monte Carlo Simulations. *Appl. Phys. Lett.* **2014**, *104*, 143104.
33. Minnich, A. J.; Johnson, J. A.; Schmidt, A. J.; Esfarjani, K.; Dresselhaus, M. S.; Nelson, K. A.; Chen, G., Thermal Conductivity Spectroscopy Technique to Measure Phonon Mean Free Paths. *Phys. Rev. Lett.* **2011**, *107*, 095901.
34. Siemens, M. E.; Li, Q.; Yang, R.; Nelson, K. A.; Anderson, E. H.; Murnane, M. M.; Kapteyn, H. C., Quasi-Ballistic Thermal Transport from Nanoscale Interfaces Observed Using Ultrafast Coherent Soft X-Ray Beams. *Nat Mater* **2010**, *9*, 26-30.
35. Touloukian, Y. S.; Ho, C. Y., *Thermophysical Properties of Matter: The Tprc Data Series. Vol. 5: Specific Heat of Nonmetallic Solids*; IFI/Plenum: New York, 1979.
36. Maros, I., *Computational Techniques of the Simplex Method*: Boston, 2003.
37. Yang, J.; Ziade, E.; Schmidt, A. J., Uncertainty Analysis of Thermoreflectance Measurements. *Rev. Sci. Instrum.* **2016**, *87*, 014901.
38. Levinshtein, M. E.; Ruyantsev, S. L.; Shur, M. S., *Properties of Advanced Semiconductor Materials: Gan, Aln, Inn, Bn, Sic, Sige*; John Wiley & Sons, Inc., 93-148, 2001.
39. Stewart, G. R., Measurement of Low‐Temperature Specific Heat. *Rev. Sci. Instrum.* **1983**, *54*, 1-11.
40. Chen, G., *Nanoscale Energy Transport and Conversion*; Oxford University Press, ISBN: 9780195159424, 2005.